Available online at www.sciencedirect.com
SCIENCE DIRECT
Journal of Catalysis 239 (2006) 1–12
JOURNAL OF CATALYSIS
www.elsevier.com/locate/jcat

Molecular structure and catalytic activity of V_2O_5/TiO_2 catalysts for the SCR of NO by NH_3: In situ Raman spectra in the presence of O_2, NH_3, NO, H_2, H_2O, and SO_2

Ioanna Giakoumelou [a], Christina Fountzoula [b], Christos Kordulis [b], Soghomon Boghosian [a,*]

[a] *Department of Chemical Engineering, University of Patras and Institute of Chemical Engineering and High Temperature Chemical Processes (FORTH/ICE-HT), GR 26500, Patras, Greece*

[b] *Department of Chemistry, University of Patras and Institute of Chemical Engineering and High Temperature Chemical Processes (FORTH/ICE-HT), GR 26500, Patras, Greece*

Received 7 June 2005; revised 30 December 2005; accepted 12 January 2006

Available online 9 February 2006

Abstract

In situ Raman spectroscopy has been used at temperatures up to 400 °C under O_2, NH_3/N_2, H_2/N_2, $NH_3/NO/O_2/N_2$, $O_2/H_2O/N_2$, and $SO_2/O_2/N_2$ for studying the influence of these gases on the molecular structure of V_2O_5/TiO_2 catalysts with V surface density, n_s, in the range 2.5–18.7 VO_x/nm^2. The catalyst activities for the SCR of NO by NH_3 have been determined to derive structure–activity relationships in combination with the Raman data. Isolated monovanadates and polyvanadates are formed at various proportions (depending on the loading) on the catalyst surface under dehydrated conditions. The band positions and characteristics are discussed in terms of possible configurations for the dispersed VO_x species. The bands observed, the surface composition, and the bond conservation rule allow to propose a small size for the V–O–V chains of polyvanadates (i.e., 2, 3). The reducing action of NH_3 is favored in the presence of adjacent V sites; at low loadings, the presence of NH_3 has no effect on the structural properties of surface VO_x. The reducibility in H_2 follows an opposite trend and is favored at low n_s, as indicated by both in situ Raman and H_2-TPR. The SO_2 presence affects only the molecular structure of catalysts with low n_s, for which a significant part of surface TiO_2 sites are vacant; the effect (judged from the in situ Raman data) is merely one of driving the dispersed vanadia species in a state of "virtually" high surface density by crowding them together, thereby providing more adjacent V sites for activation of NH_3 in SCR reaction conditions. The NO TOF values initially increase with increasing n_s, suggesting that the number of active sites per V atom increases with increasing n_s below monolayer. The formation of adjacent V–O–Ti sites is favored either at increasing n_s or at conditions of "virtually" high n_s (in the presence of SO_2). The increase in the number of such centers per V atom correlates with the increase in TOF values with increasing n_s.

Keywords: V_2O_5/TiO_2 catalysts; SCR of NO by NH_3; Molecular structure; Vanadium active sites; In situ Raman spectra; Active phase–support interactions; Effect of SO_2

1. Introduction

The emission of NO_x and sulfur oxides is responsible for the acid rain and the urban smog, which are major ecological problems. The most widely adopted process for NO_x abatement is their selective catalytic reduction (SCR) by NH_3 in the presence of O_2 over vanadia catalysts supported on TiO_2 (anatase) [1]. The literature abounds in studies related to catalytic activity, reaction mechanism, effects of vanadia loading, effects of active phase composition, effects of the support, kinetics, and so on, as has been reviewed [2,3]. Proposed SCR mechanisms suggest that NH_3 is activated and reacts from a strongly adsorbed state with gaseous or weakly adsorbed NO [2]. The differentiation of molecular structures (monooxo/polyoxo and monomeric/polymeric vanadates) in V_2O_5/TiO_2 catalysts studied by in situ Raman and IR spectroscopy has received particular attention [4,5]. It is believed that reliable structure–activity relationships can be based on the understanding of the cata-

* Corresponding author.
E-mail addresses: bogosian@iceht.forth.gr, bogosian@terpsi.iceht.forth.gr (S. Boghosian).

0021-9517/$ – see front matter
doi:10.1016/j.jcat.2006.01.019

lyst molecular structure under *operating* conditions [6,7]. The debate on the nature of active sites, although far from finalized, has resulted in reports of significant fundamental insights. Thus, a dual-site mechanism involving a surface vanadia redox site and an adjacent nonreducible site appears more favorable [8–10]. Furthermore, the reported influence of specific oxide supports, along with the observed stability of terminal V=^{18}O bonds during SCR reaction [10], suggests that the V–O–support bond is involved in the rate-determining step. Likewise, it has been shown [11] that the SCR activity of transition metal oxides supported on TiO_2 correlates well with the extent of interactions between the active phase and the support.

The vast majority of in situ Raman studies of V_2O_5/TiO_2 SCR catalysts in the literature pertain to spectra obtained under dehydrated conditions, pointing to the presence of multiple structures of surface vanadia species on TiO_2, including monomeric and polymeric vanadyl species at submonolayer coverage [11,12]. Whereas few Raman studies have examined the effect of H_2O(g) [12,13], Raman studies of V_2O_5/TiO_2 catalysts under SCR or reducing (NH_3) conditions are scarce [14, 15]. Finally, to our best knowledge, there has been no previous Raman report studying the effect of the presence of SO_2/O_2 on the molecular structure of the surface vanadia species. The lack of such studies is surprising, considering that the SO_2 presence in the gas feed during the SCR reaction over V_2O_5/TiO_2 catalysts results in an increase of TOF at low vanadia coverage [16] and that the SO_2 oxidation is undesirable during the SCR reaction [17,18]. In an attempt to begin remedying this situation, recently we have been concerned with in situ Raman studies of V_2O_5-based catalysts in $SO_2/O_2/H_2O$ atmosphere, particularly with the supported molten salt sulfuric acid catalyst, as well as vanadia/silica catalysts [19,20].

The present study focuses on the molecular structure and catalytic properties of V_2O_5/TiO_2 catalysts under SCR reaction conditions at temperatures between 250 and 450 °C. The in situ Raman spectra obtained under O_2, NH_3, and reaction ($NH_3/NO/O_2/N_2$) conditions, combined with spectra obtained under $O_2/H_2O/N_2$, $SO_2/O_2/N_2$, and H_2/N_2, provide useful information on the response of the catalyst surface to the various gases at the molecular level. This information, combined with the catalytic results, contributes to a better understanding of the behavior of the materials under study.

2. Experimental

2.1. Catalyst preparation

Anatase (SAKAI, 98%), calcined at 500 °C for 20 h, was used as carrier. Vanadium was deposited on the TiO_2 surface by wet impregnation using a vanadium oxalate aqueous solution. Water was removed slowly (over 4 h) in a rotary evaporator, and the solid thus obtained was dried at 110 °C for 5 h and calcined at 500 °C for 20 h in air. The samples are denoted as TiV_x, where x indicates their V content expressed in mol%.

2.2. Catalyst characterization

The S_{BET} and pore volume measurements were carried out in a Micromeritics ASAP 2000 apparatus at −196 °C, using N_2 as adsorption gas. X-ray diffraction patterns were obtained in the range of 0–100 °C in a Huber Imaging Plate Guinier Camera 670, which provides a high analysis diffractogram, (0.005° 2θ) with a 0.83°/min scanning rate. The sample in powder form was illuminated with Cu-K_α ($\lambda = 1.5405981$ Å) radiation.

The TPR experiments were performed in equipment described previously [21], following the ideas of the Rogers–Amenomiya–Robertson arrangement [22]. A 0.01-g sample was placed in a quartz reactor, and the gas mixture (H_2/Ar: 5/95 v/v) was passed through it for 2 h at a flow rate of 40 cm^3/min at room temperature. Then temperature was increased to 950 °C with a constant rate of 10 °C/min. Reduction led to a decrease of the H_2 concentration of the gas mixture, which was detected by a TCD detector. The reducing gas mixture was dried in a cold trap (−95 °C) before reaching the TCD.

2.3. Catalytic tests

Catalytic tests were carried out in a continuous-flow tubular fixed-bed microreactor. The reaction mixture consisted of 800 ppm NO, 800 ppm NH_3, 4% O_2, and the balance N_2. The experimental procedures, the reactor, and detector equipment used for undertaking the catalytic tests were as described previously [23].

2.4. In situ Raman spectra

Approximately 150 mg of each catalyst was pressed into a wafer and mounted on an adjustable holder of the in situ cell [19]. The gases used were O_2 (L'Air Liquide, 99.995%), 10,000 ppm NH_3/N_2 and 10,000 ppm NO/N_2 mixtures (L'Air Liquide), a 13,000 ppm SO_2/N_2 mixture (Union Carbide), a 4.3% H_2/N_2 mixture (L'Air Liquide), and N_2 (L'Air Liquide 99.999%) as balance gas, mixed using mass flow meters. The gas feed consisted of 2000 ppm NO, 2200 ppm NH_3 (NH_3/NO ratio = 1.1), 2000 ppm SO_2, 2% O_2, and 4.3% H_2 balanced in N_2, or various mixtures of these, at a total feed flow rate of 50 cm^3/min. To study the effect of H_2O(g) in the in situ Raman spectra, the dry feed gas was enriched by 8% H_2O(g) as described previously [19].

The 488.0-nm line of a Spectra Physics Stabilite 2017 Ar^+ laser was used for recording the Raman spectra. The laser beam, operated at 25 mW, was focused on the sample by a cylindrical lens to "disperse" it, to reduce sample irradiance. The scattered light was collected at 90°, analyzed with a 0.85 m Spex 1403 double monochromator, and detected by a −20 °C cooled RCA PMT equipped with EG&G photon-counting electronics.

Recording of spectra started typically at 100 °C in N_2 (hydrated conditions), after which each sample was oxidized for 1 h at 400 °C in pure O_2. Raman spectra were then recorded sequentially in O_2, NH_3/N_2, $NH_3/NO/N_2$, $NH_3/NO/O_2/N_2$, and O_2 (reoxidation) at 400, 250, and 100 °C after 1 h of gas treatment. Separate sequences were run in $O_2/N_2/H_2O$, SO_2/N_2,

$SO_2/O_2/N_2$, and O_2 (reoxidation) at 400, 250, and 100 °C after 1 h of treatment. In some cases (e.g., to check the reportedly slow interaction of SO_2 with the catalysts [24]), exposure to the gas feed was extended up to ∼20 h. Finally, to assess the reducibility of the catalysts, separate in situ Raman spectra were recorded in H_2/N_2.

3. Results and discussion

3.1. Texture and XRD

An overview of the basic characteristics of the prepared catalyst materials is given in Table 1. A diminution of both the specific surface area and the pore volume occurred, due to the deposition of V species on the TiO_2 surface. This can be attributed to the closing of the relatively narrow pores, as indicated by the corresponding pore size distribution curves, which became narrower and shifted to higher average diameters after the addition of vanadia phase. The calculation of VO_x surface density (referred to hereinafter as n_s) for each sample was based on the S_{BET} values. Monolayer surface coverage determined from Raman data is reportedly around 7–8 VO_x/nm^2 [25].

Table 1
Catalyst samples, composition, B.E.T. specific surface area (S_{BET}), pore volume (PV), surface density TOF (250 °C) of catalysts studied

Catalyst	V:Ti atomic ratio	V_2O_5 (wt%)	S_{BET} (m^2/g)	PV (cc/g)	VO_x surface density, n_s (VO_x/nm^2)	TOF ($mol_{NO\ converted}$/(V s)) at 250 °C
TiV_0	0:100	0.0	70.0	0.361	0	
TiV_2	2:98	2.4	64.0	0.350	2.5	7.5×10^{-3}
TiV_4	4:96	4.7	55.0	0.312	5.7	13.3×10^{-3}
TiV_6	6:94	6.9	42.4	0.297	10.8	8.1×10^{-3}
TiV_8	8:92	9.0	31.8	0.276	18.7	5.5×10^{-3}

As far as TiO_2 phases are concerned, only the diffraction lines of anatase appear in the XRD patterns shown in Fig. 1, indicating that neither the deposition of vanadia nor the further treatment (drying, calcination) changed the titania phase, at least in a detectable way. The catalysts with submonolayer VO_x densities (TiV_2 and TiV_4) show only the anatase peaks (Fig. 1). The absence of V_2O_5 peaks does not exclude the formation of V_2O_5 crystallites at very low concentrations or with crystallite size <40 Å. Indeed, our in situ Raman spectra described later provide evidence for the formation of such crystallites on the surface of TiV_4. Low-intensity peaks due to V_2O_5 are observed for TiV_6 and TiV_8 (Fig. 1), which have a much higher VO_x density than that exhibited by a monolayer.

3.2. In situ Raman spectra of V_2O_5/TiO_2 catalysts under various gas atmospheres

3.2.1. Oxidized catalysts—dehydrated conditions

Raman spectra for the TiV_x catalyst samples at 400 °C under flowing O_2 were in agreement with previous reports [10] and are not shown here for brevity. Instead, to analyze the structural characteristics of the dispersed vanadate species, we subtracted the contribution of the TiO_2 support from the spectra of the TiV_x samples; the resulting spectra are shown in Fig. 2. The spectra of all TiV_x samples are characterized by a well-defined band at 1026–1031 cm^{-1} (blue shifting with increasing n_s [10]) and a broad feature in the 900–940 cm^{-1} region. Two additional features are observed for TiV_6 and TiV_8 at ∼1016 cm^{-1} and at 993 cm^{-1} (strong and sharp band).

The spectra obtained for the TiV_2 (Fig. 2a) and TiV_4 (Fig. 2b) samples (with n_s of 2.5 and 5.7 VO_x/nm^2, respectively) show that vanadia occurs as both isolated monovanadates and in polyvanadate domains. The well-defined band at 1026–1031 cm^{-1} is due to the V=O stretching mode of

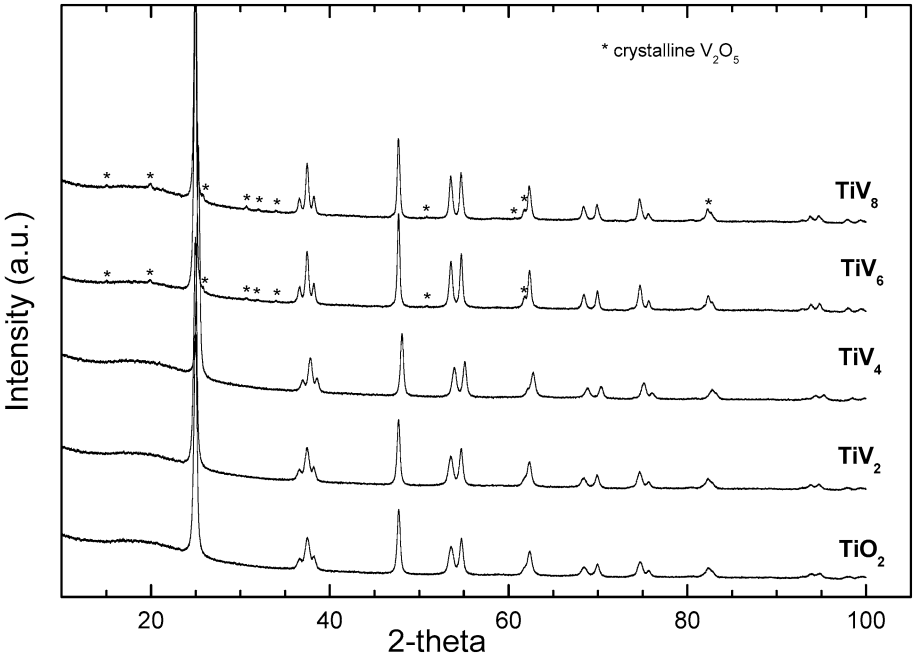

Fig. 1. X-ray diffractograms of TiV_x (V_2O_5/TiO_2) catalysts (*: V_2O_5 peaks).

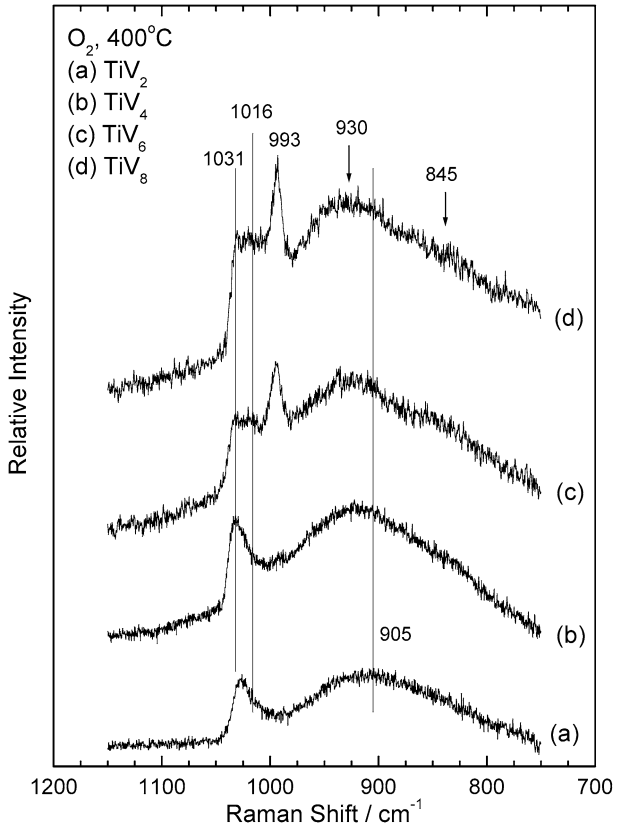

Fig. 2. In situ Raman spectra of TiV_x catalysts recorded under O_2 at 400 °C after the subtraction of the support (TiO_2) spectrum: (a) 2 mol% V (TiV_2); (b) 4 mol% V (TiV_4); (c) 6 mol% V (TiV_6); and (d) 8 mol% V (TiV_8). Laser wavelength, $\lambda_0 = 488.0$ nm; laser power, $w = 25$ mW; scan rate, sr = 0.03–0.5 cm^{-1}/s, spectral slit width, ssw = 8 cm^{-1}.

dispersed vanadia species, which at low loadings occur predominantly as isolated monovanadates in a distorted tetrahedral configuration with one short V=O terminal bond and three anchoring V–O–Ti bonds [O=V(–O–Ti)$_3$] with a near-C_{3v} symmetry [4,5,12,26,27]. But the presence of the broad band at 900–940 cm^{-1} already in spectrum a in Fig. 2 of TiV_2 is indicative of the presence of polyvanadates as well, because it is well known that a broad band at this location represents a wide set of configurations arising from V–O stretching modes within polyvanadate structures, such as V–O–V modes [4,5,12, 25–27].

The sharp band at 993 cm^{-1} observed for TiV_6 and TiV_8 (spectra c and d in Fig. 2) is due to crystalline V_2O_5 formed on the surface of these catalysts with n_s exceeding that of the monolayer. Furthermore, the same samples (with n_s of 10.8 and 18.7 VO_x/nm^2) exhibit a band at ∼1016 cm^{-1} that occurs in the V=O stretching region and is assigned to the corresponding mode of dispersed polyvanadates forming a close packing on the surface [28], thus justifying the red shift from ∼1030 to ∼1016 cm^{-1}.

In summary, the following observations can be made:

(a) The center of the broad V–O–V band occurs at 905 cm^{-1} for TiV_2 and is gradually blue-shifted at 920 cm^{-1} for TiV_4 and at ∼930 cm^{-1} for TiV_6 and TiV_8, in agreement with previous findings [28].

(b) The intensity of the same broad band increases relative to the V=O band at 1026–1031 cm^{-1} on going from TiV_2 to TiV_4 and TiV_6, indicating a higher population of dispersed polyvanadates with increasing loading, as expected.

(c) The band at ∼1016 cm^{-1} is already present in spectrum a in Fig. 2 of TiV_2 as a shoulder.

(d) A significant portion of dispersed vanadia also occurs at the surface of the low-n_s TiV_2 in the form of polyvanadates.

(e) With increasing loading (TiV_6), apart from the appearance of the V_2O_5 band at 993 cm^{-1}, the band at ∼1016 cm^{-1} becomes more intense and better resolved, indicating a larger amount of polymeric species with vanadyl units in close proximity to each other [28].

(f) A peak mass located at ∼845 cm^{-1} appears in spectra c and d in Fig. 2 of TiV_6 and TiV_8, as also observed previously [28].

(g) The presence of traces of V_2O_5 at the surface of TiV_4 is indicated by the weak band at 993 cm^{-1} seen in spectrum b in Fig. 2.

The bond lengths and bond orders of terminal V=O, bridging V–O–V, and anchoring V–O–M bonds in monovanadate and polyvanadate species can be estimated from the following formulae derived from an examination of a large number of compounds [29]:

$$\nu = 21{,}349\exp(-1.9176R) \tag{1}$$

and

$$\mathrm{BO} = \left[0.2912\ln(21{,}349/\nu)\right]^{-5.1}, \tag{2}$$

where ν is the vibrational wavenumber (cm^{-1}), BO is the bond order, and R is the V–O bond length (Å). Eqs. (1) and (2) can be used in conjunction with Raman data to check the consistency of proposed coordinations and assignments, with the constraint that the sum of BO of V–O bonds involving a particular V(V) atom should be 5 valence units (vu).

Thus, checking the case of the isolated tetrahedral monomer O=V–(O–Ti)$_3$, configuration **A** in Fig. 3, the V=O band at 1026 cm^{-1} (spectrum a in Fig. 2 of TiV_2) corresponds to a bond order of 1.89, and the remaining 3.11 vu for the three V–O–Ti bonds give rise to a BO close to unity (1.04 vu) for each V–O–Ti. In turn, according to Eq. (2), the V–O frequency along the anchoring V–O–Ti bridge can be estimated at ∼685 cm^{-1}. However, this mode is expected to be very weak in the Raman [5] and in any case would have been obscured under the wing of the very strong 630 cm^{-1} anatase band.

The dispersed polyvanadates are formed by corner-sharing of VO_4 units. Thus, each V atom in a polymeric species has one terminal V=O bond; one, two or three V–O–V bonds; and two, one or zero V–O–M bonds, where M is the metal atom of the oxide support [30,31]. The starting point of our elaboration is the 1016–1030 cm^{-1} V=O bond of polyvanadates, which corresponds to a BO of 1.85–1.89. Now, a dimeric unit can occur in two possible configurations, **B** and **C** (Fig. 3). Thus (checking the consistency of configuration **B**), the 905–930 cm^{-1} band

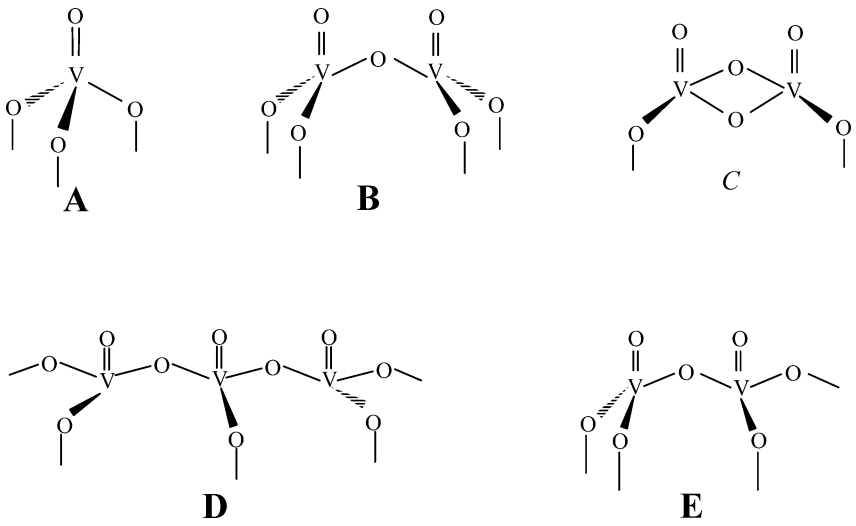

Fig. 3. Structural models for monomeric (**A**), dimeric (**B** and **C**) and polymeric (**D** and **E**) dispersed surface vanadate species.

assigned to V–O stretch along V–O–V corresponds to a BO of 1.53–1.60 [Eq. (2)], and the remaining valence units for the two V–O–Ti bonds (determined from the constraint on the total bond order for the V atom) correspond to ∼0.8 vu for the V–O bond along each anchoring V–O–Ti. Configuration **C** can be possible only when the V–O bonds along the V–O–V bridges are weaker, because if there are *two* V–O–V bonds per V (with the BO of each V–O in the range of 1.53–1.60), then there remains no vu residue for the V–O–Ti bond. Significantly, if the ∼845 cm^{-1} band (which is also in the V–O–V expected range, with a V–O BO of 1.37) is assigned to the V–O–V functionalities of configuration **C**, then there remain ∼0.4 vu for the V–O along V–O–Ti ($5 - 1.87 - 2 \times 1.37 = 0.39$). The same analysis would hold for a V atom of a chain in configuration **D**, shown in Fig. 3 (also having two V–O–V and one V–O–Ti per V).

The above elaboration points to a very low probability for the existence of two-dimensional dispersed polyvanadates (i.e., with three V–O–V per V) at the surface of the studied V_2O_5/TiO_2 catalysts. If there were three V–O–V bridges per V, then this would result in a violation of the valence sum rule, because the total sum of bond order would equal $1.87 + (3 \times 1.37) = 6$. Thus, it can be proposed that the majority of the surface dispersed polyvanadates are mainly dimeric or oligomeric species, in the sense that there is a high population of V atoms to which corresponds only one V–O–V.

It is evident that the broadness of the 845–930 cm^{-1} band is due to a wide distribution of V–O bond orders along V–O–V bridges of the dispersed polyvanadates, which occur in a number of configurations as described earlier. Furthermore, there are differences among V–O bond orders along V–O–Ti anchoring bridges between isolated monovanadates and polyvanadate domains; the observed decrease in BO on going from configuration **A** (in Fig. 3) to **B** and **C**, **D** is consistent with a corresponding lower extent of interaction between the active phase and the support. Finally, the observed strengthening of the V–O–V bonds with increasing n_s (gradual shift of 905–930 cm^{-1}) is indicative of a higher population of dimeric species with configuration **B** (in agreement with previous findings [28]) and a corresponding weakening of the anchoring bonds with increasing n_s.

3.2.2. *In situ Raman spectra under NH_3/N_2 and H_2/N_2 atmospheres*

In situ Raman spectra were obtained for the TiV_x catalysts under 2200 ppm NH_3/N_2 and 4.3% H_2/N_2. First, we explore the effect of NH_3 on the catalyst molecular structure at various loadings; second, to discriminate between the reducing action and the chemisorption of NH_3 we compare the in situ Raman spectra under NH_3 to the corresponding spectra obtained under H_2.

Ammonia can influence the surface of the catalysts under study in at least in two ways, by being chemisorbed on their surface or by reducing V^{5+} after being activated on the surface. The chemisorption can occur either on vacant Ti^{4+} Lewis acid centers of TiO_2 or on coordinatively unsaturated V atoms. Fig. 4 shows the in situ Raman spectra of the TiV_x catalysts under flowing NH_3 at 400 °C. In the presence of NH_3, the signal-to-noise ratio decreased, indicating a progressively stronger absorption of the incident laser beam. Comparing the spectra in Fig. 4 and the corresponding spectra obtained under O_2 reveals the following findings:

(a) Spectrum b (Fig. 4) of TiV_2 obtained under NH_3 shows no difference compared with the corresponding spectrum obtained under O_2 (shown in Fig. 9Aa), indicating that at low VO_x surface densities, NH_3 is selectively chemisorbed on vacant Ti^{4+} Lewis acid sites of the carrier without affecting the molecular structure of dispersed vanadia [14,15].

(b) With increasing n_s, the 1026 cm^{-1} V=O band of TiV_x catalysts under NH_3 undergoes a *red shift* (1026 → 1024 → ∼1004 → ∼1000 cm^{-1}, on going from TiV_2 to TiV_8), in contrast to the blue shift (1026 → 1031 cm^{-1}) observed in the spectra of TiV_x/O_2 with increasing n_s (Fig. 2), indicating a structural perturbation resulting from the coordination of NH_3 to the dispersed vanadia species.

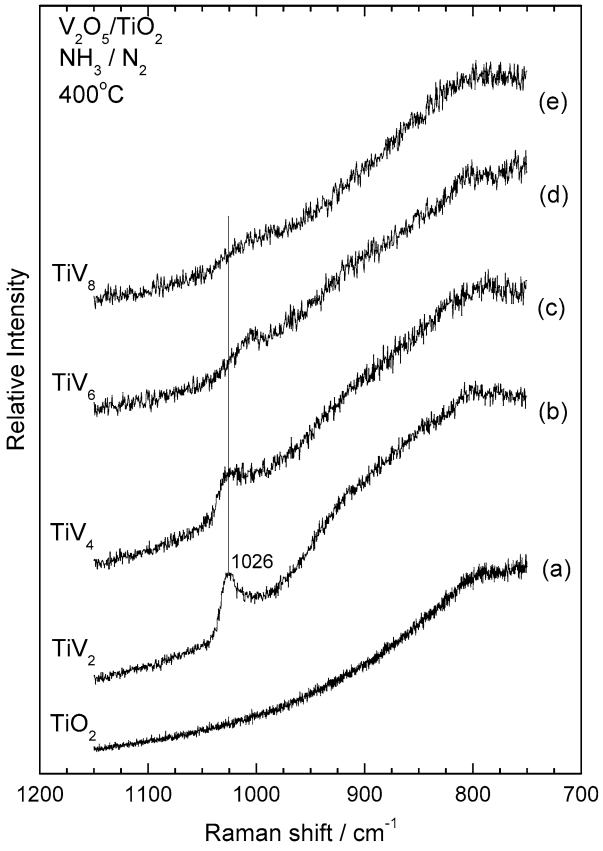

Fig. 4. In situ Raman spectra of the TiV_x catalysts recorded under NH_3/N_2 atmosphere at 400 °C: (a) TiO_2; (b) TiV_2; (c) TiV_4; (d) TiV_6 and (e) TiV_8. Recording parameters: see Fig. 2 caption.

(c) Both V=O and V–O–V bands lose intensity with increasing loading, indicating a removal of oxygen and reduction that occurs to a larger extent with increasing n_s.
(d) The 993 cm^{-1} V_2O_5 band is absent from spectra d and e (Fig. 4) of TiV_6 and TiV_8, in which the surface density exceeds that of the monolayer, indicating a complete reduction of crystalline V_2O_5 by NH_3.

Thus, it appears that the activation of NH_3 to act as a reducing agent is favored by the presence of V centers in high densities; that is, the presence of adjacent V sites favors the reduction of V^{5+} by NH_3. This fits well with the observed increase of TOF for the SCR of NO by NH_3 over vanadia catalysts with increasing n_s for surface densities below monolayer [16], a behavior also observed in the present work and discussed below.

Catalyst reducibility was studied by H_2-TPR; the TPR profiles of pure TiO_2 and TiV_x catalysts are shown in Fig. 5. The experimental protocol used resembles that used for the characterization of Eurocat V_2O_5/TiO_2 catalysts by TPR [32]. The TPR profiles have the same shape, consisting of a main peak followed by a "shoulder" at higher temperatures. The onset of H_2 consumption is shifted to higher temperatures with increasing loading, starting from below 400 °C for TiV_2 and TiV_4. The maximum of the main peak is shifted to higher temperatures (from 435 °C for TiV_2 to 540 °C for TiV_8), whereas the temperature maximum for the shoulder also increases from 510 °C for TiV_2 to 590 °C for TiV_8. To compare the TPR profiles of Fig. 5 to those reported previously [32], we need to take into account that the S_{BET} of the TiO_2 carrier in the present work is almost seven times greater than that used for the Eurocat samples. With this in mind, the TPR profile obtained for TiV_8 (Fig. 5e) compares very well to the profile obtained for the Eurocat sample with corresponding dispersion (sample EL10V1).

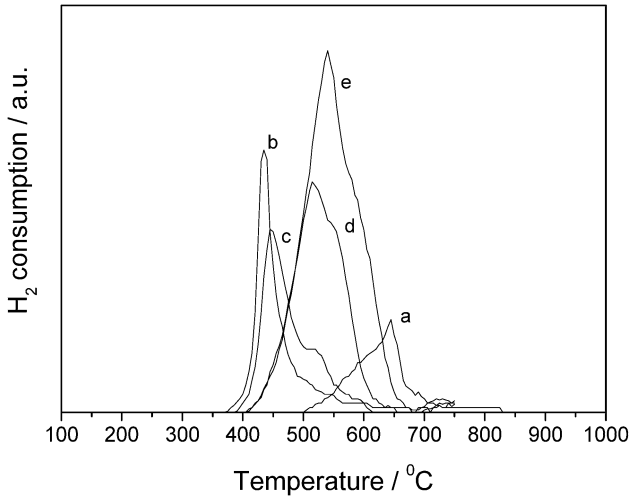

Fig. 5. H_2-TPR profiles for TiV_x catalysts: (a) TiO_2; (b) TiV_2; (c) TiV_4; (d) TiV_6 and (e) TiV_8.

The TPR profiles show that there are at least two kinds of surface-dispersed vanadium species in samples with submonolayer coverage: (a) species with strong support–active phase interaction predominating at low loadings that are easily reduced by H_2 and (b) species with weaker support–active phase interaction (polymeric groups with weak V–O–Ti anchoring bridges, vide supra) that are reduced at higher temperatures. The reduction of V_2O_5 crystallites occurs at even higher temperatures; it is known that bulk V_2O_5 is reduced around 600 °C and that the rate of reduction of V_2O_5 microcrystallites increases with decreasing crystal width along the c axis [33]. Finally, from the H_2 consumption, it turns out that a complete reduction of V^{5+} to V^{3+} has occurred.

The in situ Raman spectra of the TiV_x catalysts under 4.3% H_2/N_2 at 400 °C (Fig. 6) confirm the observations of the H_2-TPR measurements. The 1026 cm^{-1} (V=O) and 905–930 cm^{-1} (V–O–V) bands disappear from spectra a and b (Fig. 6) of TiV_2 and TiV_4, showing that dispersed vanadia is completely reduced, in agreement with the respective TPR profiles showing the onset of H_2 consumption for $T < 400$ °C for these samples. With increasing n_s and accumulation of polymeric species (and correspondingly lower order of anchoring V–O–Ti bonds as proposed above), the reduction by H_2 is more difficult (Fig. 6c for TiV_6), in agreement with the TPR profiles. Finally, the V_2O_5 crystallites "survive," as indicated by the presence of the 993 cm^{-1} band in spectra c and d (Fig. 6) of TiV_6 and TiV_8, and it was necessary to increase the temperature to 470 °C and expose TiV_8 to 4.3% H_2/N_2 for another 1 h to achieve complete reduction of all surface vanadia species (Fig. 6e).

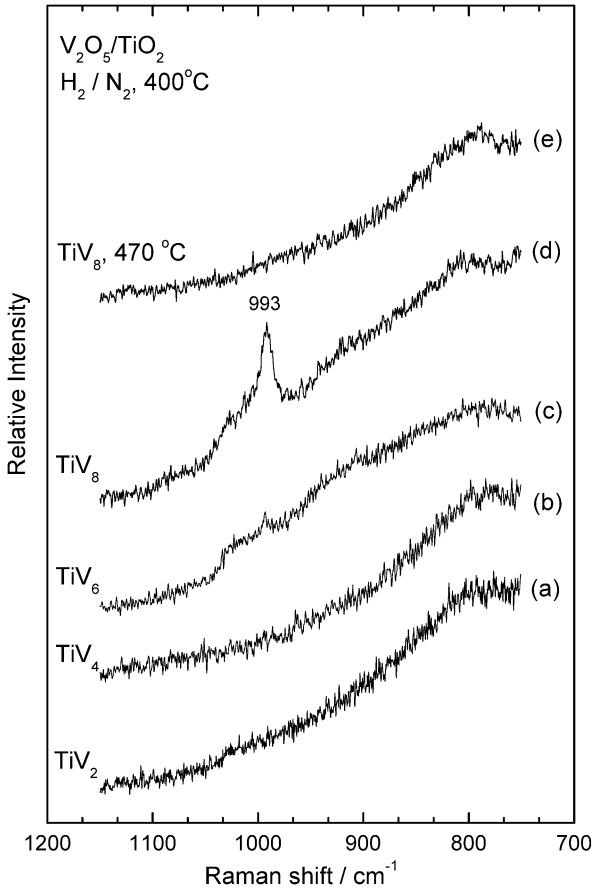

Fig. 6. In situ Raman spectra of the TiV_x catalysts recorded under H_2/N_2 atmosphere at 400 °C: (a) TiV_2; (b) TiV_4; (c) TiV_6; (d) TiV_8 and (e) TiV_8 at 470 °C. Recording parameters: see Fig. 2 caption.

3.2.3. *In situ Raman spectra under SCR conditions ($NH_3/NO/O_2/N_2$ atmosphere)*

After recording the spectra in NH_3 atmosphere, an NO stream was mixed with the gas feed to obtain a 2200-ppm NH_3/2000-ppm NO/N_2 mixture. Then in situ Raman spectra were recorded after exposing the catalysts to $NH_3/NO/N_2$ atmosphere for 1 h. Subsequently, the gas feed was enriched with 2% O_2, and spectra were recorded after exposure to $NH_3/NO/O_2/N_2$ atmosphere for 1 h. Fig. 7 shows the series of sequential in situ Raman spectra obtained as above for TiV_2 and TiV_6. The presence of NO did not affect the spectra obtained under NH_3. On addition of O_2 to the $NH_3/NO/N_2$ feed, the band intensities due to dispersed monomeric and polymeric V species, as well as due to crystalline V_2O_5, were reinstated and became similar to those seen under oxidizing conditions. Obviously, O_2 (being an accelerator of the SCR reaction) reoxidizes surface vanadia and drastically lowers the extent of the interaction of NH_3 with the surface vanadia species at steady state.

3.2.4. *Effect of $H_2O(g)$ in the molecular structure of V_2O_5/TiO_2 catalysts*

The effect of $H_2O(g)$ in catalyst activity has attracted interest, because in many cases $H_2O(g)$ is present in the catalyst environment either in the feed or as a product. The presence

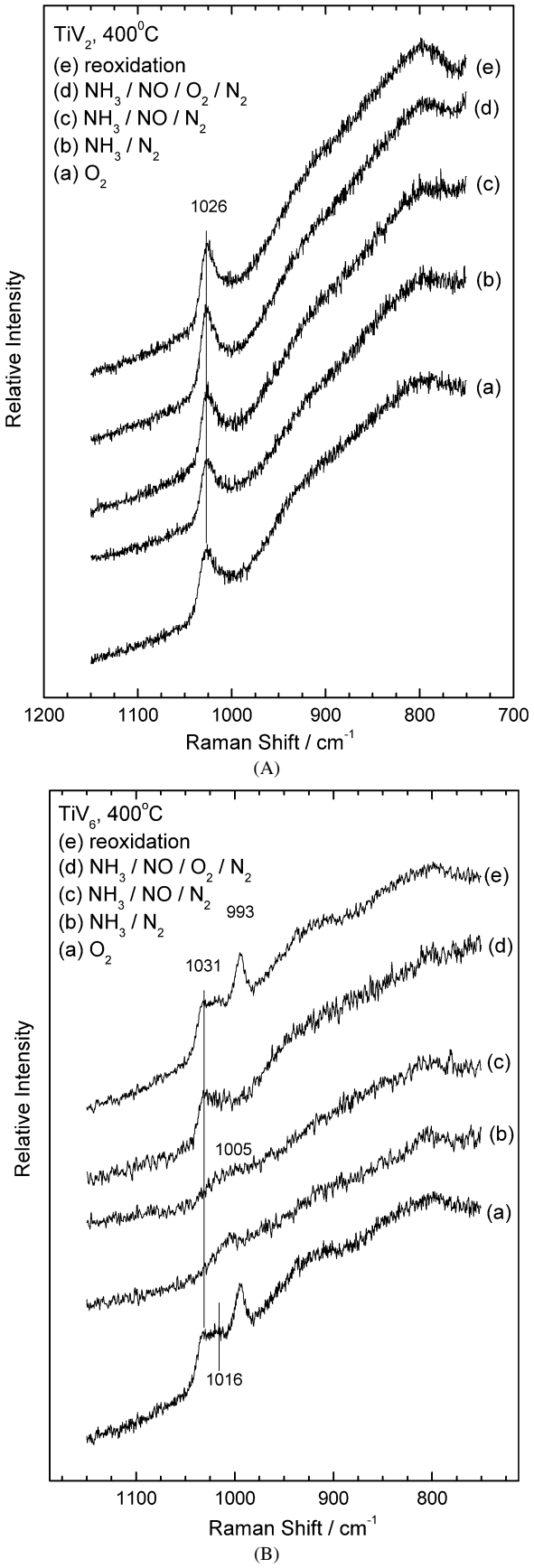

Fig. 7. In situ sequential Raman spectra of TiV_2 and TiV_6 catalysts recorded at 400 °C under various $NH_3/NO/O_2/N_2$ atmospheres as indicated by each spectrum. Recording parameters: see Fig. 2 caption.

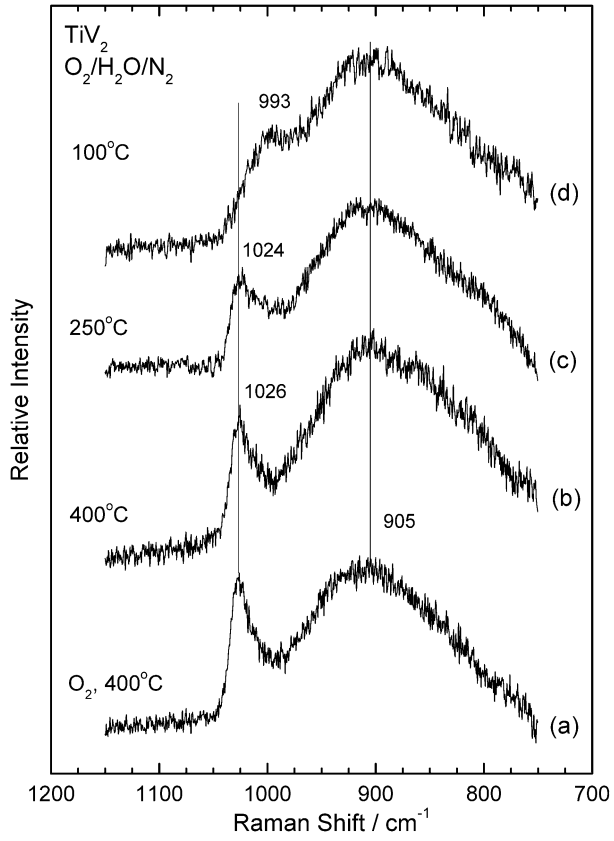

Fig. 8. In situ Raman spectra of TiV_2 catalyst (after the subtraction of the support (TiO_2) spectrum) recorded at temperatures and atmospheres as indicated by each spectrum: (a) under O_2 atmosphere at 400 °C; (b–d) under $H_2O/O_2/N_2$ atmosphere at 400–250–100 °C. Recording parameters: see Fig. 2 caption.

of H_2O(g) can affect the extent of surface hydroxylation, the distribution of Brønsted and Lewis acid sites on the catalyst surface, and the molecular structure of the dispersed surface metaloxides. However, under in situ conditions, adsorbed water is thermally desorbed, and the surface metaloxide layers are dehydrated.

The effect of H_2O(g) was studied by comparing the dehydrated Raman spectra with those obtained under the presence of H_2O(g). Our observations are in full agreement to those reported previously [13] and are presented briefly. Fig. 8 shows the in situ sequential Raman spectra obtained for the TiV_2 after subtraction of the spectrum of the TiO_2 carrier; the sequences for the other samples are omitted for brevity. First, each sample was heated at 400 °C under O_2 and its spectrum was recorded. Then the gas feed was enriched with 8% H_2O(g), and the in situ spectrum was recorded under 2% O_2/8% H_2O/N_2 sequentially at 400, 250, and 100 °C after exposing the sample to the feed gas for 1 h.

At 400 °C, H_2O(g) had no effect on the positions, relative intensities, and shapes of the bands due to dispersed vanadates, which remain unchanged compared with the corresponding bands of the dehydrated spectra. However, H_2O(g) can still influence the kinetics and/or yield of the reaction, because H_2O is a product of the SCR reaction. At 250 °C, the V=O band lost intensity and broadened; this effect was more intense at 100 °C, where the V=O band was replaced by a broad feature at ∼993 cm^{-1}.

Table 2
Observed Raman band wavenumbers (cm^{-1}) for the most common V–O modes of dispersed vanadia in representative V_2O_5/TiO_2 catalysts under the influence of various gas atmospheres at 400 °C

Sample/ n_s	V–O mode	O_2	NH_3	H_2	H_2O/O_2	SO_2/O_2
TiV_2/	V=O	1026	1026	–	1026[b]	1031
2.5 V/nm^2	V–O–V	905	905	–	905[b]	905[c]
TiV_6/	V=O	1031	1004[a]	1031[a]	1031[b]	1031
10.8 V/nm^2		1016	–	1016[a]	1016[b]	1016
	V–O–V	930	915[a]	930[a]	930[b]	930

[a] Bands with low intensities, indicative of reduction of V and removal of oxygen due to NH_3 or H_2 action.

[b] The presence of H_2O perturbs the V–O bands to an extent that becomes observable in the Raman spectra at $T < 250$ °C.

[c] V–O–V band intensity increased relative to the V=O band intensity under the influence of SO_2/O_2.

Below 250 °C, the interaction of adsorbed moisture, presumably by means of hydrogen bonding with the V=O units [12], perturbs the V=O bonds by causing red shifts to the V–O bond frequency. Lowering the temperature favors the absorption and coordination of moisture to the surface vanadia species. Moreover, in the case of the TiV_2 sample with low n_s, the water molecules can also interact with the surface hydroxyls and cause hydration to an extent that can cause flooding of the surface. Such an extensive surface hydration can lead to hydrolysis of the anchoring V–O–Ti bonds for the TiV_2 sample, and the resulting molecular structure of the surface vanadia at low temperatures (e.g., 100 °C) will resemble the structure of $V_{10}O_{28}^{6-}$, in which the V=O band is at 990 cm^{-1}. In contrast, for samples with higher loadings (with coverages near or above monolayer), the water molecules interact solely with the dispersed surface vanadia species.

3.2.5. *In situ Raman spectra under $SO_2/O_2/N_2$ atmosphere*

The study of V_2O_5/TiO_2 catalysts in the presence of SO_2 is important because SO_2 is a flue gas constituent and has a reported beneficial effect in the TOF of these materials for the SCR of NO by NH_3 at low V surface densities [16]. The presence of SO_2 has no effect in the TOF for coverages above half a monolayer [16]. Fig. 9 shows the effect of SO_2 in the in situ Raman spectra obtained for TiV_2 (Fig. 9A) and TiV_6 (Fig. 9B) at 400 °C, with the spectra obtained under O_2 included for comparison (spectra Aa and Ba (Fig. 9)). Table 2 lists the observed Raman band wavenumbers for the various V–O modes of dispersed vanadia for TiV_2 and TiV_6 at 400 °C. The spectra in Fig. 9A show that the presence of SO_2 perturbs the molecular structure of the surface vanadia species of the TiV_2 catalyst (n_s of 2.5 V/nm^2); Fig. 10 illustrates this more clearly, showing the spectra of TiV_2 at 400 °C after subtracting the contribution of TiO_2 from the spectra of Fig. 9A. Under the presence of SO_2, the 1026 cm^{-1} V=O band is shifted to 1031 cm^{-1} (see also the inset in Fig. 10); however, the broad 905 cm^{-1} V–O–V band maintains its position but gains in intensity relative to the 1026–1031 cm^{-1} band. In contrast, the molecular structure

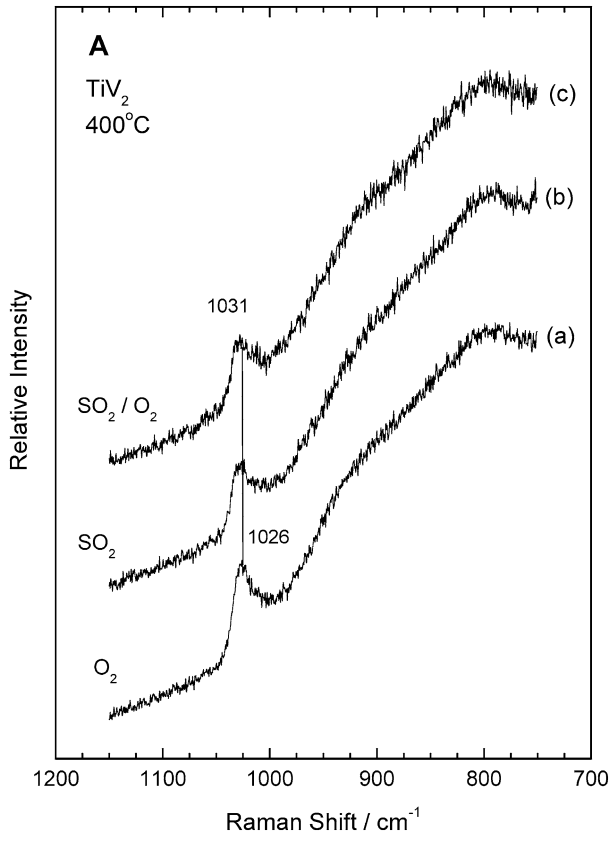

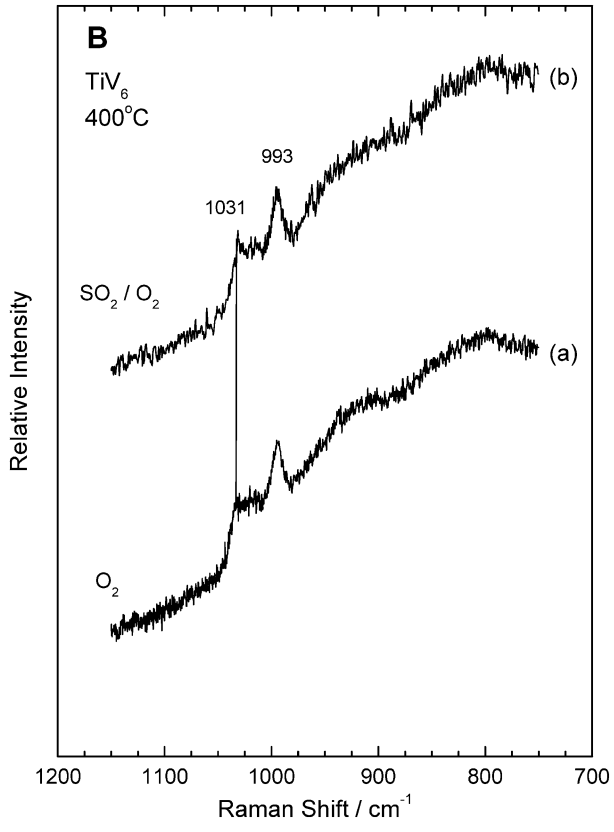

Fig. 9. In situ Raman spectra of TiV_2 (A) and TiV_6 (B) catalysts recorded under $SO_2/O_2/N_2$ atmospheres at 400 °C: (Aa) TiV_2 under O_2; (Ab) TiV_2 under SO_2/N_2; (Ac) TiV_2 under $SO_2/O_2/N_2$. (Ba) TiV_6 under O_2; (Bb) TiV_2 under $SO_2/O_2/N_2$. Recording parameters: see Fig. 2 caption.

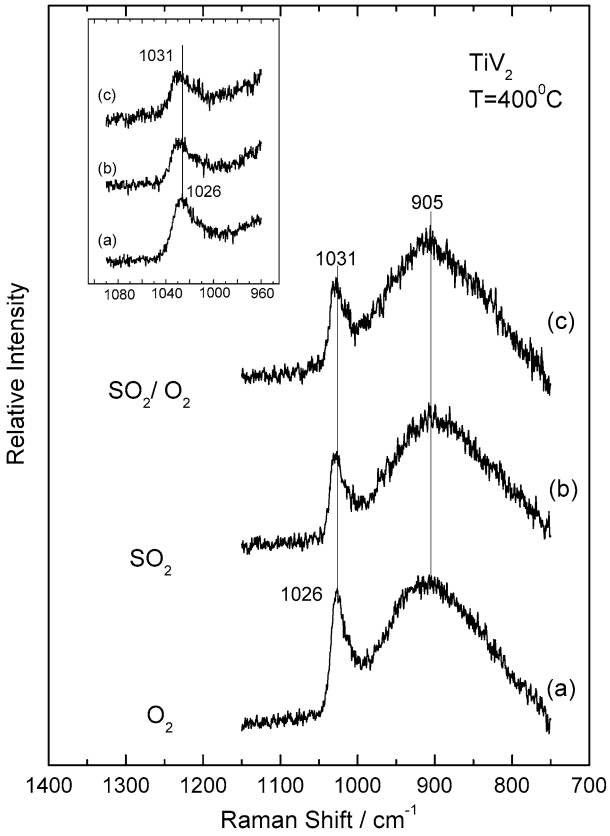

Fig. 10. In situ Raman spectra of TiV_2 catalyst recorded under $SO_2/O_2/N_2$ atmosphere after the subtraction of the support (TiO_2) spectrum, at 400 °C: (a) O_2; (b) SO_2/N_2; (c) $SO_2/O_2/N_2$. Inset: Magnification of the 1000–1050 cm^{-1} range. Recording parameters: see Fig. 2 caption.

of TiV_6 shows remarkable stability in terms of the 1031 cm^{-1} V=O and the broad 930 cm^{-1} V–O–V bands (see Fig. 9B).

It is known that the adsorption and oxidative adsorption of SO_2 in the surface of TiO_2 results in the formation of surface sulfates [34], which transform into strong Bronsted acid sites in the presence of $H_2O(g)$ [35]. The same effect can occur on the surface of V_2O_5/TiO_2 catalysts with submonolayer coverage (e.g., TiV_2) where part of the TiO_2 surface is available, thereby increasing the number of available sites for adsorption and activation of NH_3 and hence increasing the rate of the SCR reaction [16]. In contrast, it is known that <0.4% of the surface V sites of a monolayer V_2O_5/TiO_2 catalyst (~8 V/nm^2) adsorbed SO_2 during the oxidative adsorption of SO_2 at 175 °C [34]. This explains why it has not been possible in the present work to observe any association of SO_2 with the V_2O_5/TiO_2 catalysts and the stability manifested by, for instance, the TiV_6 (10.8 V/nm^2) sample under SO_2.

It is noteworthy that Dunn et al. [34] observed very low activity of V_2O_5/TiO_2 catalysts for the oxidation of SO_2 at 400 °C. Furthermore, they suggested that the active center for the oxidation of SO_2 is not a "dual site" (V–O–V), because in such a case they should observe an increasing trend in the TOFs versus n_s, at least in a certain range of loadings. In the absence of evidence for correlation between the V=O position and the catalytic activity, Dunn et al. [34] concluded that SO_2 coordinates on the anchoring V–O–Ti bond and stated that this

is supported by the fact that the TOF values versus n_s are nearly stable. However, closer inspection of their data reveals a small systematic decrease of the TOFs with increasing n_s (for submonolayer coverages), an observation that in fact validates their conclusion, because the number of anchoring V–O–Ti bonds per V is decreased with increasing n_s for submonolayer coverages as more V atoms are involved in V–O–V bridges with increasing n_s (see Fig. 3). Indeed, if the V–O–Ti centers are the active sites for the SO_2 oxidation, then a moderate decrease in TOF (activity per V) with increasing n_s would be expected Moreover, the results of the present work are consistent with a small size of polymer species from low loadings. This results in a small decrease in the number of V–O–Ti bridges per V with increasing n_s and fits well with the moderate decrease of TOF versus n_s observed previously [34] for the SO_2 oxidation.

As mentioned earlier, the molecular structure of the TiV_2 catalyst (2.5 V/nm^2) is perturbed in SO_2 atmosphere (Figs. 9A and 10). This has to do with the ability of the weakly acidic SO_2 to interact with the TiO_2 support and form sulfate groups that occupy the most basic sites of the support by "ejecting" the dispersed vanadia species, and also the ability of SO_2 to "attack" the anchoring V–O–Ti bonds [34]. In this way, the number of sites remaining available for the surface vanadia is reduced and exist in an environment of virtually high surface density in the form of congestion/crowding. This results in a higher polymer-to-monomer ratio and to an increase in the number of dual sites at low surface densities. This explains the shift of the V=O mode from 1026 to 1031 cm^{-1} (see, e.g., Fig. 10), which is a characteristic of catalysts with high n_s (Fig. 2) and also justifies the increased intensity of the broad V–O–V band relative to the V=O for the TiV_2 catalyst in SO_2/O_2 atmosphere (Fig. 10). Moreover, crowding of the dispersed vanadia species will result in formation of multiple pairs of adjacent V–O–Ti sites, as the various units are being confined in congested regions. Finally, the establishment of conditions of "virtually" high surface densities at low loadings with the subsequent formation of additional adjacent V sites also explains the reported threefold increase in TOFs for the SCR of NO by NH_3 in the presence of SO_2 for catalysts with low (up to approximately half a monolayer) surface densities [16].

3.3. Catalytic activity

Catalyst performance has been evaluated in terms of NO conversion (shown in Fig. 11), NH_3 consumption, and N_2 yield in the temperature range of 250–450 °C. NO conversion increases with loading up to 4 mol% V and then decreases for all temperatures. The temperature at which the maximum NO conversion is achieved is different for each catalyst and decreases with loading. The percent NH_3 consumption coincides with the percent NO conversion at 250 and 300 °C and follows the same trend as seen for percent NO conversion. Maximum values for the yield in N_2 were achieved at 350 °C for TiV_4, TiV_6, and TiV_8 and at 450 °C for TiV_2.

To gain insight into the intrinsic activity of VO_x entities in the SCR of NO, the values obtained at 250 °C were used for calculating TOF [$\text{mol}_{\text{NO converted}}/(\text{mol}_{\text{V}}\ \text{s})$]; the results are listed

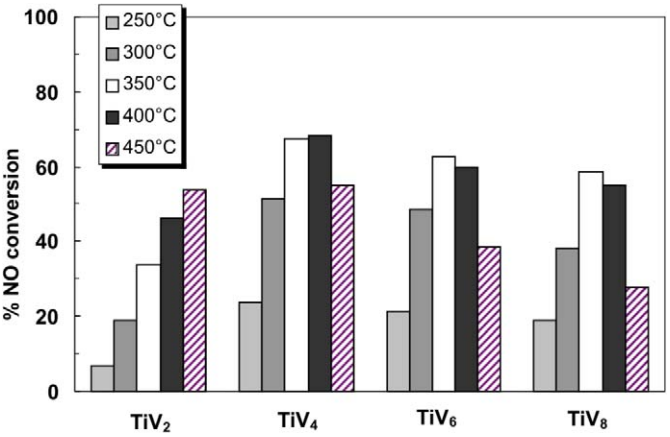

Fig. 11. % NO conversion for TiV_x catalysts, measured at 250–450 °C.

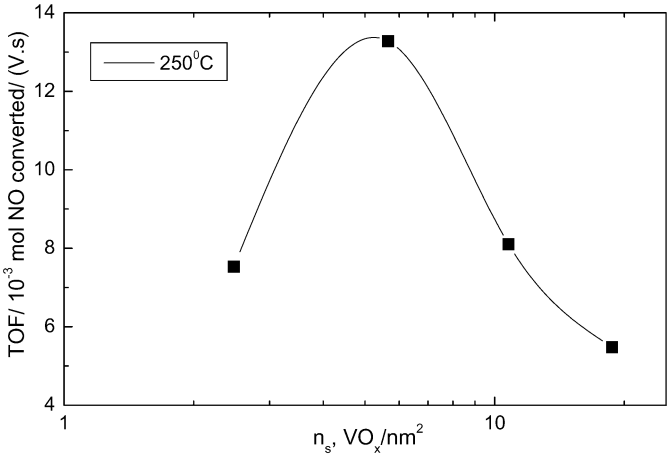

Fig. 12. TOF values ($\text{mol}_{\text{NO converted}}/(\text{mol}_{\text{V}}\ \text{s})$) for the SCR of NO by NH_3 (NH_3/NO = 1/1, $W/F = 0.0012$ g s/cm^3) as a function of VO_x surface density, n_s (VO_x/nm^2) for the TiV_x catalysts, calculated at 250 °C.

in Table 1 and plotted in Fig. 12. These values were calculated after verifying that at 250 °C, the reactor performance was differential. Fig. 12 shows that the TOF increased with increasing n_s for loadings corresponding to coverages lower than that of a monolayers, in agreement with previous reports [15,16]. Furthermore, Amiridis et al. [16] showed that the increase of TOF versus n_s occurs for coverage up to approximately half a monolayer. The decrease in TOF values for samples with n_s exceeding the monolayer (TiV_6 and TiV_8) is due to the formation of V_2O_5 crystals not 100% dispersed on the surface, as required for the TOF calculations.

3.4. On the active site for the SCR of NO by NH_3 and structure–activity relationships

The behavior of TOF versus n_s (Fig. 12) is considered typical for V_2O_5/TiO_2 catalysts for the SCR of NO by NH_3 [10,16]. The initial increase is indicative of a higher activity of V centers, of which the formation is favored with increasing n_s. These centers could include units that contain V–O–V bridges because the number of V–O–V bridges per V increases with increasing n_s at low loadings as more V atoms are incorporated in V–O–V

bridges, as well as adjacent units with V–O–Ti sites in close proximity to each other with increasing n_s, thereby increasing the number of V–O–Ti sites adjacent to another V′–O–Ti site per V. Both of these structural transformations can be correlated to the increase of TOF, which is also expressed per V.

With reference to the observed trends in TOF versus n_s, we can make the following remarks:

(a) If the TOFs were independent on n_s, then we would have an indication of "single active sites" of which the number per V atom would be stable (independent on n_s). The V=O site is an example of such a site; regardless of the degree of polymerization, there is always one V=O per V.
(b) If the TOFs were decreasing with increasing n_s, then the activity would be linked to sites of which the number per V atom is decreasing with increasing n_s. The anchoring V–O–Ti is an example of such a site; the number of anchoring V–O–Ti bonds per V decreases with increasing n_s due to the incorporation of V in V–O–V bridges (see Fig. 3).

Thus, the results of the present work suggest that the active V center is a "dual site" involving probably a V–O–V bridge or pairs of adjacent V–O–Ti sites, the formation of which is favored with increasing loading at low surface densities, as described above. In particular, the increase in TOF (activity per V) cannot be justified only by the emergence of V–O–V bridges with increasing n_s. The number of V–O–V bridges per V is 0 for monomeric units, 0.5 for dimeric units, and 0.67 for trimeric units (see Fig. 3); however dimeric and/or trimeric units exist already from low loadings, and therefore the increase in TOF (almost twofold in Fig. 12 and in earlier work [16]) cannot be justified only by the incorporation of V in V–O–V bridges. In contrast, the number of pairs of adjacent V–O–Ti bridges (with different V atoms in neighboring units) may very well increase with increasing n_s, and this increase correlates with the increase in TOF. This is further justified by the effect of SO_2, which drives dispersed vanadia species to congestion (in a form of crowding) and creates such pairs of adjacent V–O–Ti sites. The proposed importance of pairs of adjacent V–O–Ti sites as the active centers for the SCR of NO by NH_3 is also based on the reported influence of oxide supports combined with ^{18}O substitution studies [10] and the good correlation between catalytic activity and extent of interactions exerted between the active phase and the support surface [11], suggesting that the anchoring V–O–support bond is involved in the rate-determining step. Moreover, there is no correlation between the position and/or the intensity of the 1026–1031 cm^{-1} V=O band with the TOF values, which is in agreement with literature findings excluding the V=O centers from being the active sites for the SCR of NO by NH_3, although the active centers (whatever they are) have, as a matter of course, a terminal V=O.

The increase of TOF versus n_s for coverages below monolayer has previously been ascribed to high specific activity of polymeric vanadate species [15], an increased number of Brønsted acid sites associated with the presence of vanadium on the surface [8,9], and the requirement of two adjacent active sites for the SCR reaction [9,10].

4. Conclusion

The molecular structure and catalytic properties of V_2O_5/TiO_2 catalysts with densities 2.5–18.7 V/nm^2 were studied for the SCR of NO by NH_3 at 250–450 °C. The fully oxidized catalyst surface under dehydrated conditions exhibits two types of dispersed vanadia: isolated monovanadates and polyvanadates at various proportions, depending on the vanadium surface density, n_s. The bands observed, the surface composition, and the bond order conservation rule allow us to propose the existence of small V–O–V polyvanadate chains (e.g., 2, 3). At low loadings, NH_3 does not affect the molecular structure of dispersed surface vanadia species (apparently being preferentially chemisorbed on vacant titania sites); the perturbation and reduction of dispersed vanadia by NH_3 is favored by the presence of adjacent V sites at high (e.g., $n_s > 5$ V/nm^2) surface densities. Catalyst reducibility in H_2 follows an opposite trend and is favored at low n_s, where strong support–active-phase interactions predominate. The presence of SO_2 (with or without O_2 present) results in a blue-shift (by 5 cm^{-1}) of the V=O band and an increased intensity due to V–O–V functionalities for catalysts with low n_s, indicating that the adsorption and oxidative adsorption of SO_2 on vacant carrier sites drives the dispersed vanadia in a state of "virtually" high surface density by crowding the V sites, thereby providing more adjacent V sites for activation of NH_3 in SCR reaction conditions in the presence of SO_2. The reactivity studies showed that the TOF values initially increase with increasing n_s, confirming that the reaction is accelerated for submonolayer coverages in the presence of adjacent V sites. This result indicates that the number of active sites per V atom increases with increasing n_s for submonolayer coverage. Such centers could be either V–O–V units or (most likely) pairs of adjacent V–O–Ti sites created from the formation of dispersed vanadates in close proximity to each other.

Acknowledgments

Financial support was provided by the Research Committee of the University of Patras (C. Caratheodory grant for basic research).

References

[1] H. Bosch, F.J.J.G. Janssen, Catal. Today 2 (1988) 369.
[2] G. Busca, L. Lietti, G. Ramis, F. Berti, Appl. Catal. B: Environ. 18 (1998) 1.
[3] V.I. Parvulescu, P. Grange, B. Delmon, Catal. Today 46 (1998) 233.
[4] G. Busca, J. Raman Spectrosc. 33 (2002) 348.
[5] M. Banares, I. Wachs, J. Raman Spectrosc. 33 (2002) 359.
[6] B.M. Weckhuysen, Chem. Commun. (2002) 97.
[7] G. Garcia-Corttez, M.A. Banares, J. Catal. 209 (2002) 197.
[8] N.-Y. Topsøe, H. Topsøe, J.A. Dumesic, J. Catal. 151 (1995) 226.
[9] N.-Y. Topsøe, J.A. Dumesic, H. Topsøe, J. Catal. 151 (1995) 241.
[10] I.E. Wachs, G. Deo, B.M. Weckhuysen, A. Andreini, M.A. Vuurman, M. de Boer, M.D. Amiridis, J. Catal. 161 (1996) 211.
[11] K. Bourikas, Ch. Fountzoula, Ch. Kordulis, Appl. Catal. B: Environ. 52 (2004) 145.
[12] G.T. Went, S.T. Oyama, A.T. Bell, J. Phys. Chem. 94 (1990) 4240.
[13] J.-M. Jehng, G. Deo, B.M. Weckhuysen, I.E. Wachs, J. Mol. Catal. A: Chem. 110 (1996) 41.

[14] G.T. Went, L.-J. Leu, S.J. Lombardo, A.T. Bell, J. Phys. Chem. 96 (1992) 2235.
[15] G.T. Went, L.-J. Leu, R.R. Rosin, A.T. Bell, J. Catal. 134 (1992) 492.
[16] M.D. Amiridis, I.E. Wachs, G. Deo, J.-M. Jehng, D.S. Kim, J. Catal. 161 (1996) 247.
[17] J.P. Dunn, H.G. Stenger Jr., I.E. Wachs, Catal. Today 51 (1999) 301.
[18] J.P. Dunn, H.G. Stenger Jr., I.E. Wachs, J. Catal. 181 (1999) 233.
[19] A. Christodoulakis, S. Boghosian, J. Catal. 215 (2003) 139.
[20] I. Giakoumelou, V. Parvulescu, S. Boghosian, J. Catal. 225 (2004) 337.
[21] N. Spanos, H.K. Matralis, Ch. Kordulis, A. Lycourghiotis, J. Catal. 136 (1992) 432.
[22] J.L. Lemaitre, in: F. Delaney (Ed.), Characterization of Heterogeneous Catalysts, Dekker, New York/Basel, 1984.
[23] Ch. Fountzoula, H.K. Matralis, Ch. Papadopoulou, G.A. Voyiatzis, Ch. Kordulis, J. Catal. 184 (1999) 5.
[24] C. Orsenigo, A. Berreta, O. Forzatti, J. Svachuyla, E. Troconi, F. Bregani, A. Baldacci, Catal. Today 27 (1996) 15.
[25] I.E. Wachs, B.M. Weckhuysen, Appl. Catal. A 157 (1997) 67.
[26] I.E. Wachs, Catal. Today 27 (1996) 437.
[27] A. Christodoulakis, M. Machli, A.A. Lemonidou, S. Boghosian, J. Catal. 222 (2004) 293.
[28] G.T. Went, L.-J. Leu, A.T. Bell, J. Catal. 134 (1992) 479.
[29] F.D. Hardcastle, I.E. Wachs, J. Phys. Chem. 95 (1991) 5031.
[30] S.C. Su, A.T. Bell, J. Phys. Chem. B 102 (1998) 7000.
[31] B.M. Weckhuysen, D.E. Keller, Catal. Today 78 (2003) 25.
[32] R.A. Koeppel, J. Nickl, A. Baiker, Catal. Today 20 (1994) 45.
[33] F. Roozeboom, M.C. Mittelmejer-Hazeleger, J.A. Moulijn, J. Medema, V.H.J. de Beer, P.J. Gellins, J. Phys. Chem. 84 (1980) 2783.
[34] J. Dunn, P.R. Koppula, H.G. Stenger, I.E. Wachs, Appl. Catal. B: Environ. 19 (1998) 103.
[35] J.P. Chen, R.T. Yang, J. Catal. 139 (1993) 277.